This is an open access article published under a Creative Commons Non-Commercial No Derivative Works (CC-BY-NC-ND) Attribution License, which permits copying and redistribution of the article, and creation of adaptations, all for non-commercial purposes.

ACS SENSORS

ACS AUTHORCHOICE

pubs.acs.org/acssensors

Article

Nanodiamond Relaxometry-Based Detection of Free-Radical Species When Produced in Chemical Reactions in Biologically Relevant Conditions

Felipe Perona Martínez,[§] Anggrek Citra Nusantara,[§] Mayeul Chipaux,* Sandeep Kumar Padamati, and Romana Schirhagl*

Cite This: *ACS Sens.* 2020, 5, 3862−3869

Read Online

ACCESS | Metrics & More | Article Recommendations | Supporting Information

ABSTRACT: Diamond magnetometry is a quantum sensing method involving detection of magnetic resonances with nanoscale resolution. For instance, T1 relaxation measurements, inspired by equivalent concepts in magnetic resonance imaging (MRI), provide a signal that is equivalent to T1 in conventional MRI but in a nanoscale environment. We use nanodiamonds (between 40 and 120 nm) containing ensembles of specific defects called nitrogen vacancy (NV) centers. To perform a T1 relaxation measurement, we pump the NV center in the ground state (using a laser at 532 nm) and observe how long the NV center can remain in this state. Here, we use this method to provide real-time measurements of free radicals when they are generated in a chemical reaction. Specifically, we focus on the photolysis of H_2O_2 as well as the so-called Haber−Weiss reaction. Both of these processes are important reactions in biological environments. Unlike other fluorescent probes, diamonds are able to determine spin noise from different species in real time. We also investigate different diamond probes and their ability to sense gadolinium spin labels. Although this study was performed in a clean environment, we take into account the effects of salts and proteins that are present in a biological environment. We conduct our experiments with nanodiamonds, which are compatible with intracellular measurements. We perform measurements between 0 and 10^8 nM, and we are able to reach detection limits down to the nanomolar range and typically find T1 times of a few 100 μs. This is an important step toward label-free nano-MRI signal quantification in biological environments.

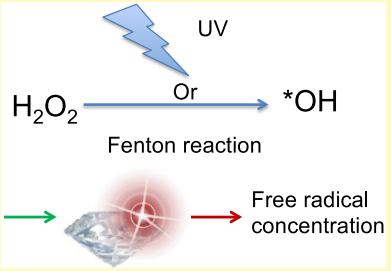

KEYWORDS: *nitrogen vacancy center, ODMR, biochemical analysis, hydroxyl radical, magnetometry, relaxometry*

Color defects in diamonds have been studied intensively as novel and powerful (quantum) magnetometers.[1] This field has also attracted attention in other disciplines, including biology[2] and geoscience,[3] or for industrial applications.[4−6] Due to its nearly infinite photostability, the nitrogen vacancy (NV) defect in diamond has been presented as an attractive label for cellular structures.[7,8] Additionally, nanodiamonds show excellent biocompatibility in all kinds of cell types[9] and organisms.[10]

Arguably more remarkable, however, is the NV center's ability to sense magnetic resonances optically. It does so by changing its brightness based on the magnetic surroundings. The technique is so sensitive that the faint magnetic resonance of a single electron[11] or even a few nuclear spins[12,13] can be detected experimentally. This effect has already been utilized for several different applications, including characterizing magnetic vortices,[14] hard drives,[15,16] nanoparticles,[17] single proteins,[18] or different chemicals as fluorinated compounds.[19]

One particularly interesting sensing scheme is the so-called relaxation (or T1) measurements, which are sensitive to spin fluctuations. This pulsing scheme, which only requires optical pulsing, has already been used successfully to determine the concentration of spin labels,[20] copper ions,[21] temperature,[22] or conductivity.[23] Sushkov et al. demonstrated single-molecule sensitivity when determining the concentration of gadolinium-containing molecules attached to a diamond surface.[24] Kaufmann et al. achieved gadolinium determination in lipid bilayers.[25] In addition to detecting spin labels in water, Steinert et al. demonstrated the first nano-magnetic resonance imaging (MRI) with this technique from a fixed slice of a cell embedded in a polymer.[20] The cell was prepared similarly to samples for electron microscopy but stained with gadolinium.

For the first time, we determined free-radical concentrations in situ during a chemical reaction. We were able to measure a low concentration of *OH radicals (2 μmol) that are naturally present in living cells. We generated them from an H_2O_2 precursor either by UV radiation or by applying iron ions with the Haber−Weiss reaction.

There are a couple of indicators for hydroxyl radicals,[26] which can be used directly in cells or in solution, but diamond

Received: May 22, 2020
Accepted: November 20, 2020
Published: December 3, 2020

© 2020 American Chemical Society

https://dx.doi.org/10.1021/acssensors.0c01037
ACS Sens. 2020, 5, 3862−3869

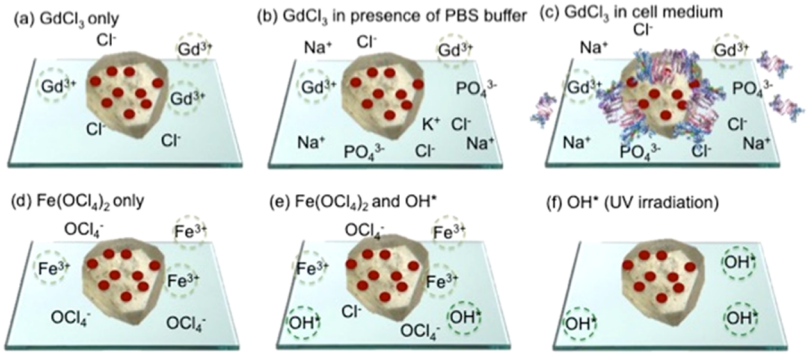

Figure 1. Overview of the samples in this article. The experiments in the first line aim to measure (a) $GdCl_3$ in water, (b) $GdCl_3$ in PBS, and (c) $GdCl_3$ in cell culture medium. The goal of these experiments is to determine the influence of salts and cell medium proteins on the sensing ability of NV center ensembles in nanodiamonds. The lower half of the figure represents measurements of naturally occurring species that give a magnetic resonance signal. In (d), $Fe(OCl_4)_2$ is measured in water, and in (e), H_2O_2 is added to $Fe(OCl_4)_2$, which leads to the generation of *OH radicals. In each experiment, the compound that causes the signal is measured is circled in green dotted lines.

magnetometry offers additional advantages. Fluorescent labels (some of which are used here for direct comparison) react with reactive species and are converted into fluorescent compounds in the process. However, they suffer from bleaching, and thus continuous measurements are not possible. Additionally, the label is consumed in the reaction, making the sensing process irreversible. Diamond relaxometry allows for better spatial and temporal resolution as well as the ability to repeat the measurement over time without destruction of the probe or killing the cell.

Additionally, we perform calibration measurements with known concentrations of gadolinium to directly compare different sensing conditions. Figure 1 summarizes the investigated conditions. For the first time, we take the presence of salts and proteins into account. We investigated different effects by comparing the T1 responses to gadolinium under various conditions. Moreover, we considered the effect of the size of the nanodiamonds on the T1 relaxation constant.

EXPERIMENTAL SECTION

Nanodiamonds. The nanodiamonds used in the experiments were ground HPHT diamonds of different sizes, which are commercially available from Adamas Nanotechnology. As a last step of the manufacturing process, these materials are cleaned with an oxidizing acid and thus have an oxygen-terminated surface. They are also irradiated by the manufacturer and contain NV centers in a proportion of 2 ppm (approximately 15 NV centers per particle) for 40 nm diamonds, 2.5 ppm (approximately 300 NV centers per particle) for 70 nm diamonds, and 3 ppm for 120 nm diamonds (approximately 1000 NV centers per particle). To produce a homogeneous distribution of nanodiamonds on the bottom of a glass-bottom cell culture dish, 100 μL of a suspension of fluorescent nanodiamonds (0.1 $\mu g\ mL^{-1}$) was poured into the dish, and then the medium was removed. To perform a measurement, new medium containing the analyte needs to be added. NV centers only detect analytes within a distance of a few nanometers. This means that in principle, only a very small sample volume is needed. However, it is important to either avoid evaporation of the medium during the measurement or use sufficiently large sample volumes. For the samples, we added 200 μL of water, phosphate-buffered saline (PBS), cell medium (Dulbecco's modified Eagle's medium (DMEM) complete), gadolinium chloride solution or iron(II) perchlorate solution. No special sample preparation was required.

T1 Measurements. We used a homemade confocal microscope to localize our nanodiamonds. An Olympus UPLanSApo40× NA = 0.95 air objective collects their photoluminescence, which is then selected through a 550 nm long-pass filter and a confocal pinhole. Light is finally detected by an avalanche photodiode (SPCM-AQRF-15-FC) in single photon counting mode. More information on the equipment can be found in an article by Morita et al.[27] For our measurements, we excluded obvious aggregates. We also chose particles with counts between 10^6 and 10^7 counts/s and relaxation times between 90 and 300 μs. Extreme values were excluded since they were either from dirt particles on the surface, aggregates or background or exceptionally large or small particles. T1 relaxation measurements were conducted. The NV centers were polarized by a train of laser pulses with variable dark times (from 0.2 μs to 10 ms). The laser (532 nm, CNI, Changchun, China) was attenuated to 100 μW ($2 \times 10^5\ W\ cm^{-2}$) at the location of the sample. To ensure the polarization of the NV centers, the pulse length was set to 5 μs. The photoluminescent signal (PL, detected above 550 nm) was quantified in a detection window of 0.6 μs. To ensure an adequate signal-to-noise ratio, we repeated the sequence shown in Figure 2a 10 000 times. Each sequence consisted of 30 dark times (τ). The resulting measurement time was approximately 8 min. These parameters were used in each T1 relaxometry experiment. The T1 relaxation curve was fitted with a biexponential function, and the reported T1 constant is the higher time constant yield by fitting (eq 1).

$GdCl_3$ Sensitivity in Different Media/Conditions. To prepare a stock solution, gadolinium(III) chloride (Aldrich 439770-5G) was dissolved in MQ water, phosphate-buffered saline (PBS), or cell medium to a concentration of 1 M, starting with the control sample (100 μL of solvent). Before the measurement, the $GdCl_3$ solution was added gradually to give the desired concentrations (0.001 μM, 0.01 μM, 0.1 μM, 1 μM, 10 μM, 100 μM, 1 mM 10 mM, and 100 mM). T1 measurements were recorded at each concentration according to the procedure described above. The experiments were repeated with four different particles.

Hydrogen Peroxide and UV Light. Hydrogen peroxide 30% was purchased from Sigma-Aldrich. *OH radicals are generated by photolysis of hydrogen peroxide stimulated by UV light (275 nm, 23.7 mW cm^{-2}). The relaxation constant T1 was recorded with and without exposure to UV light. The particles were exposed to UV radiation during the complete acquisition time, which was approximately 17 min. The results were calculated from a dataset composed of eight nanodiamonds.

A set of similar experiments was conducted with the objective of building a calibration curve. This curve shows the relationship between the concentration of *OH and T1. To change the concentration of *OH in the solution, we diluted 30% H_2O_2 to 20 and 10%, and as in the previous experiment, we exposed the solutions to UV light while measuring the T1 value. The curve was built from a dataset of seven different nanodiamonds.

Measuring the Hydroxyl Radical by Hydroxyphenyl Fluorescein (HPF). To validate our results, we repeated the same experiments that we performed with T1 measurements with HPF.

https://dx.doi.org/10.1021/acssensors.0c01037
ACS Sens. 2020, 5, 3862−3869

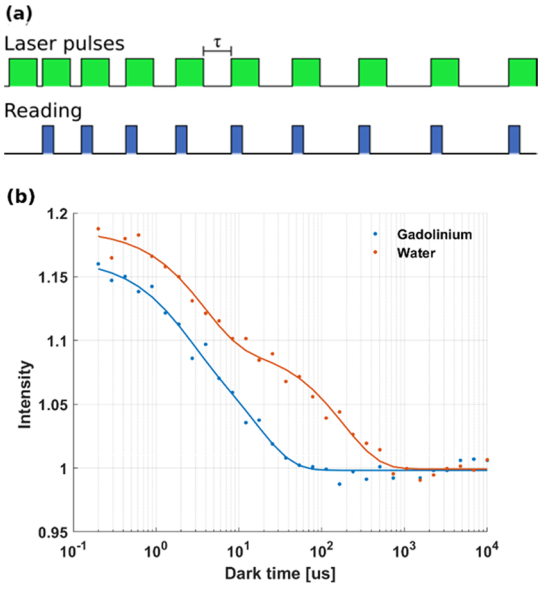

Figure 2. T1 measurements: (a) pulsing sequence to generate a T1 curve. The green rectangles indicate when the laser is on, while the blue rectangles indicate when we read out. The green bars are separated by a dark time τ. This dark time is systematically increased. Plotting the different dark times against the fluorescence intensity that we recorded during the blue windows results in curves shown in (b). In the presence of flipping spins, this decay is faster. This is, for example, the case when adding gadolinium. The blue curve results from adding 0.5 mM Gd^{3+}.

Hydroxyl radicals and hydroxyphenyl fluorescein (HPF) were purchased from Thermo Fisher (H36004). The experiments were conducted by following the procedure proposed by the manufacturer. The samples were prepared in a 96-well plate in sextuplets. The concentration of HPF in each well was 10 μM. Iron(II) perchlorate was added to a concentration of 100 μM, and hydrogen peroxide was added at 1 mM. The samples were excited with light at 485 nm, and the signal was quantified at 520 nm using a FLUOstar OPTIMA plate reader (BMG LABTECH). The samples were measured at intervals of 1 h for 14 h.

Measuring the Concentration of Hydroxyl Radicals by 2-Hydroxy Terephthalic Acid (HTA). This assay was used to validate our T1 data and to determine which concentration of *OH was present. 2-Hydroxy terephthalic acid (Na_2Th, Sigma-Aldrich, used without further purification) acts as a standard chemical trap for hydroxyl radicals and is a standard hydroxyl dosimeter. To determine the concentrations of *OH in our reaction and to validate our T1 results, we used iron(II) perchlorate (10 μM), H_2O_2 (1000 μM), and Na_2TH (200 μM). A calibration plot was established with different concentrations of HTA (vs) intensity using a fluorimeter (Edinburgh Instruments (module sc-20), $\lambda_{excitation}$ = 330 nm and $\lambda_{emission}$ = 420 nm). From the calibration plot, the concentration of hydroxyl radicals was determined.[28]

Measuring the Fenton Reaction by Relaxometry. Nanodiamonds (70 nm) were fixed in a glass-bottom culture dish according to the procedure described above (Nanodiamonds section). After finding a particle containing the ensemble of NVs, 180 μL of ultrapure water was added to the plate, and the first set of measurements was performed (in water only). Iron(II) perchlorate was added until a concentration of 10 μM was reached. Another set of T1 relaxometry measurements was conducted over the same ensemble of NV centers used in the previous case. H_2O_2 was incorporated into the previous solution, and a new set of measurements was taken. The same procedure was repeated with three particles.

RESULTS AND DISCUSSION

In this article, we measure and compare the spin-lattice relaxation times (T1) under biologically relevant conditions. To elicit T1, a specific pulse sequence is required, which is shown in Figure 2a. To perform the measurement, we first prepared the defects in their spin ground state. This was done by a laser pulse. Then, we measured again after specific times to see whether the NV centers were still in this "bright spin state" or in thermal equilibrium with the two other "darker" spin states. Since the states differ in brightness, we can observe the process by recording the change in fluorescence. When there are flipping spins (in this case, from gadolinium or free radicals) in the surroundings, the NV centers will lose this state faster. Thus, the time that is required to lose the prepared state gives a measure of the concentration of these species. Two typical curves taken in the presence and absence of gadolinium are shown in Figure 2b.

In principle, one can use single defects or ensembles of defects to perform diamond magnetometry measurements.[17,29] Here, we chose to use NV center ensembles hosted in nanodiamonds. Compared to single NV center measurements, this has the advantage that each particle is brighter (and thus easier to find even if there is background fluorescence). Additionally, each measurement already combines multiple NV centers. As a result, the variability between particles is smaller (see the Supporting Information).

It should be noted that the form of the curve we obtain for ensembles of NV centers is slightly different from single NVs. For a single NV, T1 relaxation can be described by two exponential models;[30] here, we observe multiple of these decays with different relaxation times at the same time. The difference in relaxation times within a particle likely results from different distances to the particle surface as well as their respective nanoscale environment. The result is a decay curve with a shoulder (see Figure 2b (water)). In our experiment, our shortest dark times were not short enough to detect the effect of relaxation through the metastable state, which is related to an initial build-up of the relaxation curve. Instead, we obtained monotonically decreasing functions.

We therefore use a different model to fit our data and extract the relaxation constant. For analysis, we approximate that the ensemble relaxation consists of two components.[31] One originates from NV centers that are very close to the surface, and another originates from NV centers that are deeper in the crystal and thus less influenced by the surface. The model used to fit the data is

$$\mathrm{PL}(\tau) = I_{\mathrm{inf}} + C_{\mathrm{a}}\, \mathrm{e}^{-\tau/\mathrm{Ta}} + C_{\mathrm{b}}\, \mathrm{e}^{-\tau/\mathrm{Tb}}$$
$$\mathrm{T1} = \max(\mathrm{Ta}, \mathrm{Tb}) \quad (1)$$

From eq 1, we obtain the constants Ta and Tb, and we defined the value of T1 as the highest constant. Longer T1 times are more sensitive to changes in magnetic noise. Generally, the longer the T1 before adding the analytes, the more it can still be reduced (see Supporting Information). Thus, we used the slower relaxation constants for analysis and quantification throughout this article. The different contrasts in the curves of Figure 2b are a consequence of two factors. First, the degree of depolarization, after the same dark time, is expected to be higher when the NV center is exposed to magnetic noise. Second, the contrast is also dependent on the pumping efficacy. Then, technical inaccuracies (such as slow fluctuations

https://dx.doi.org/10.1021/acssensors.0c01037
ACS Sens. 2020, 5, 3862−3869

in the laser power) might affect the measurement. For these reasons, we chose to calculate the relaxation time constant obtained from sampling a set of dark times instead of comparing the fluorescence intensity directly.

As reported by Manson et al.,[32] the laser may induce charge transfer to the NV centers. Similarly, spin diffusion would induce a decrease in the measured photoluminescence. First, this would generate a signal not affected by spin relaxation and thus decrease the contrast of our T1 curves (C_a or C_b). In addition, similar to the NV center spin states, the charge states have different luminescence values. As a consequence, any mechanism linking free-radical generation, as induced in this work, to the NV center charge state would affect our relaxation curve similarly. However, unlike the free-radical-induced spin relaxation that is well described in the literature, such a linkage to charge state relaxation has yet to be established.

In this work, the calibration we perform in Figures S9 and 5 allows us to link known concentrations with a specific change in T1 time regardless of its exact origin.

Performance of the NVs in Biologically Relevant Conditions. When sensing spins in a biological environment, they coexist with salts and proteins in the medium. These might cover the surface of the particle hosting the NVs.[33] To quantify chemicals in such an environment, it is important to know how these factors influence the signal from the NV centers.

We therefore performed measurements of known concentrations of gadolinium under different conditions. The aim of these measurements is to optimize the measurement conditions and understand the influence of different factors on sensing capabilities.

We tested the effects of adding salts and proteins (components of the medium) to a solution of Gd^{3+} (a common spin label). Then, we compared the performance of the NV centers in water.

$GdCl_3$ in Water. Gadolinium is one of the most common contrast agents in conventional magnetic resonance measurements. Thus, measuring gadolinium ions provides a convenient way to compare conditions and determine the influence of different factors. Measurements in water were conducted as a reference. The concentration of $GdCl_3$ was increased in steps of 1 order of magnitude from 1 nM to 100 mM. As expected, there was an inverse relationship between the relaxation constant T1 and the concentration of $GdCl_3$ (red dots in Figure 3). The signal saturated at approximately 10 μM. The lowest concentration we were able to determine was 1 nM.

Presence of Salts. PBS is the most common buffer for biological experiments. The most abundant salts present in the medium are sodium chloride (NaCl) and disodium phosphate (Na_2HPO_4). PBS is used to maintain the pH of the growth medium constant at 7.4, and it is required for cells to prevent osmotic stress. To investigate how these salts influence the sensitivity of quantum sensing, we used 70 nm nanodiamonds with ensembles of NV centers. We measured different concentrations of gadolinium trichloride ($GdCl_3$) diluted in PBS. Figure 3 (green dots) shows the results of the measurements. The measured T1 constants are close to the control sample (water), indicating that PBS does not influence the sensing performance.

Nanodiamonds Covered with a Protein Corona. In a biological medium, nanoparticles never just stand by themselves. Instead, a corona of proteins and salts surrounds them.[33] There are some ongoing efforts to avoid corona formation on nanodiamonds;[34] however, they require elaborate chemistry, and the coating that is required might influence sensing performance as well. Here, we investigate how the presence of the corona influences sensing performance. The blue points in Figure 3 show how the T1 values change as the concentration of Gd^{3+} increases. In the presence of proteins, the change in T1 is shifted toward higher concentrations. This is likely due to a shielding effect, in which the proteins attach to the surface of the nanodiamonds and thus hinder Gd^{3+} from approaching the surface. Thus, the decrease in T1 is considerably slower. Additionally, we observe a larger spread of data in the presence of the corona. Despite the dispersion of the measurements, we clearly see a reduction in the relaxation constant as the concentration of gadolinium increases. The larger spread in T1 values in the samples with protein corona is likely due to differences in the corona that is formed around each particle. The thickness and exact composition (the medium contains a mixture of thousands of proteins) of the protein corona can vary significantly.

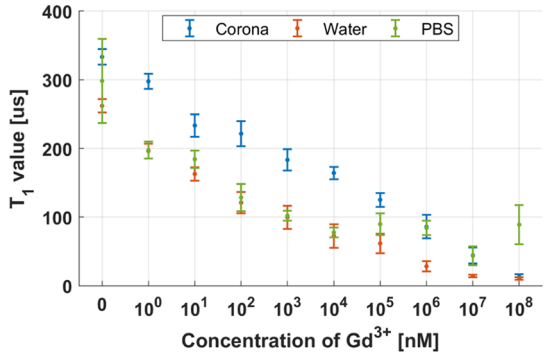

Figure 3. T1 value at several concentrations of Gd^{3+}. The gadolinium salt was diluted in three different media: water, PBS, and cell growth medium (DMEM complete). The error bars represent the standard error of the mean from six particles.

Measuring Free Radicals In Situ. *Photolysis of H_2O_2.* In two different experiments, we show the determination of hydroxyl radical concentrations produced in situ. In the first experiment, we produced *OH by photolysis of hydrogen peroxide (H_2O_2), as indicated in eq 2.

$$H_2O_2 + h\nu \rightarrow 2\ {}^*OH \tag{2}$$

To this end, the T1 constant was first measured in H_2O_2 (30%) in the dark and then with UV light on (λ = 275 nm). Finally, we also performed another measurement in the dark (after the radicals had reacted) to test the reversibility of the measurement.

To estimate the concentration of *OH during the reaction, we performed quantification with disodium terephthalic acid.[28] Na_2TA reacts with the hydroxyl radical, resulting in the formation of the fluorescent molecule HTA in a 1:1 proportion. Based on the HTA calibration plot (see Supporting Information, Figures S7–S9), we estimated a concentration of *OH radicals of 0.9 μM.

As Figure 4 shows, after initiating the photolysis reaction, the relaxation of the NV centers resulted in thermal equilibrium that was approximately 30% faster. The speedup in the relaxation (and the reduction of T1) in this case can be explained by the generation of hydroxyl radicals. Moreover, after stopping the photolysis, we observed a recovery of the initial value, indicating a reduction in the concentration of

https://dx.doi.org/10.1021/acssensors.0c01037
ACS Sens. 2020, 5, 3862−3869

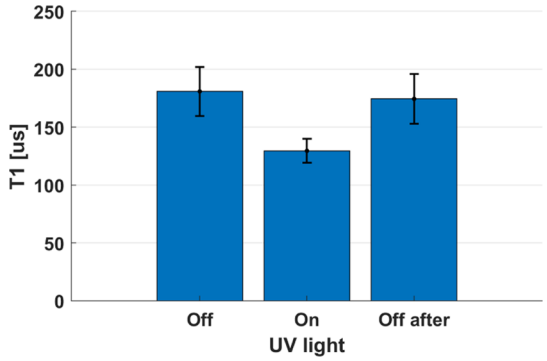

Figure 4. Determination of *OH produced by photolysis of hydrogen peroxide. The change in the T1 relaxation time after turning on UV light is explained by the emergence of 0.9 μM hydroxyl radicals. The error bars show the standard error of the mean obtained from seven different experiments with different diamonds.

radicals in the NV center near the environment. As a control, we performed the same experiment in the absence of H_2O_2. This is an important control to rule out any effects the UV irradiation might have on the NV centers themselves (for example, charge conversion, which might occur during irradiation). In the absence of H_2O_2, we observed the relaxation time to be unperturbed by UV light (see Figure S5).

The ability to sense the radical concentration in real time is specific for the NV center. To the best of our knowledge, this cannot be achieved with any other fluorescent probe to date.

T1 Calibration Curve. To understand how T1 changes with varying radical concentrations, we recorded a calibration plot. This allowed us to estimate an unknown concentration from a T1 value. According to eq 2, the amount of hydroxyl radicals produced by the exposure of H_2O_2 to UV light at a fixed UV light intensity depends on the concentration of H_2O_2 in the sample. When using NV centers for sensing radicals, this relation should be reflected in the change in T1 when the concentration of *OH changes. Figure 5 shows the result of measuring T1 at several concentrations of H_2O_2 at a fixed UV light intensity. The concentration of *OH was estimated from the results of the HTA experiment. As expected, the T1 value decreases as the concentration of *OH increases, but the relation is not linear, as might be expected from eq 2. The

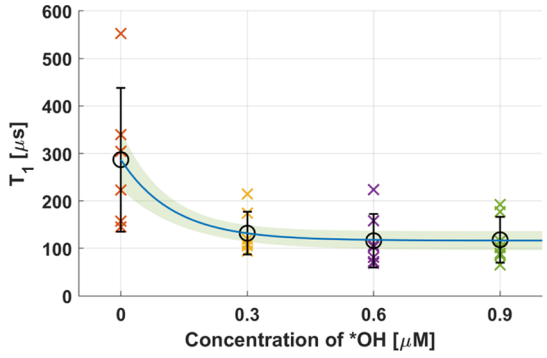

Figure 5. T1 Calibration curve. The T1 value of an ensemble of NV centers decreases exponentially (blue line) as the concentration of *OH increases. The black circles show the mean value of T1, and the error bars show the standard deviation. The green shade around the curve represents the 95% confidence interval, calculated for each concentration (±62 μs for water, ±17 μs for 0.3 μM, ±21 μs for 0.6 μM, and ±18 μs for 0.9 μM).

measurements saturate at high concentrations of H_2O_2 (over 20%).

Although this limitation exists, the concentrations of free radicals we expect to find in biological samples are several orders of magnitude lower, and saturation would not interfere with the measurements in those cases.

Figure 5 shows the empirical data obtained from the measurement of the T1 constant at different concentrations of *OH. To obtain the analytical relationship between T1 and C_{*OH} (concentration of *OH), we assumed an exponential relationship as follows

$$T1(C_{*OH}) = T1_{\infty}(1 + A\, e^{-C_{*OH}/C_0}) \quad (3)$$

where $T1_{\infty}$ is expressed in μs, C_0 is expressed in μM, and A is dimensionless.

The parameters of the model in eq 3 are calculated by a nonlinear fitting procedure. The error intervals were estimated from the standard deviation of the resulting parameters.

$T1_{\infty} =$
116.6 ± 1.05 μs
$A = 1.5 \pm 0.03$
$C_0 =$
0.12 ± 0.009 μM

Haber–Weiss Reaction. The third experiment performed to determine *OH concentrations mimicked the Haber–Weiss reaction. This is one of the pathways that cells use to produce *OH. One key step in this process is the well-known Fenton reaction,[35] which describes the oxidation of iron(II) to iron(III) by the action of hydrogen peroxide (eq 4), producing one hydroxyl radical and one hydroxide ion.

$$Fe^{2+} + H_2O_2 \rightarrow Fe^{3+} + {}^*OH + OH^- \quad (4)$$

Cellular iron is present mostly linked to other molecules, such as proteins, or chelated in the labile iron pool (LIP). Free iron (Fe(II) and Fe(III)) available in the cell can catalyze a Haber–Weiss reaction, generating oxygen, hydroxide, and highly reactive hydroxyl radicals.[36]

We reproduced this reaction and measured the radicals created. To benchmark the relaxometry performance, we ran two experiments in parallel. One uses NV centers, and another uses the reactive oxygen species probe hydroxyphenyl fluorescein (HPF). While T1 measurements are sensitive to spin noise (giving the overall concentration of radicals or paramagnetic chemicals), HPF is sensitive to *OH. The results can be seen in Figure 6. In both cases, we used ultrapure water as the negative control, and we did not expect to find a measurable trace of *OH in this sample. The second sample consisted of only the salt that provided iron(II) (iron(II) perchlorate) in ultrapure water. Finally, we started the Fenton reaction by incorporating hydrogen peroxide into the sample.

In the HPF measurement, the fluorescence intensity of HPF is proportional to the amount of *OH in the sample. In Figure 6a, it is clearly visible that the production of *OH started only after the addition of H_2O_2 to the sample. Additionally, here, we determined the concentration of *OH using Na_2TH. The amount of *OH radicals during the reaction was approximately 1.96 μM.

When using relaxometry, the T1 relaxation time already responds to iron(II) perchlorate. Then, the relaxation constant T1 is reduced even more after starting the generation of *OH.

https://dx.doi.org/10.1021/acssensors.0c01037
ACS Sens. 2020, 5, 3862–3869

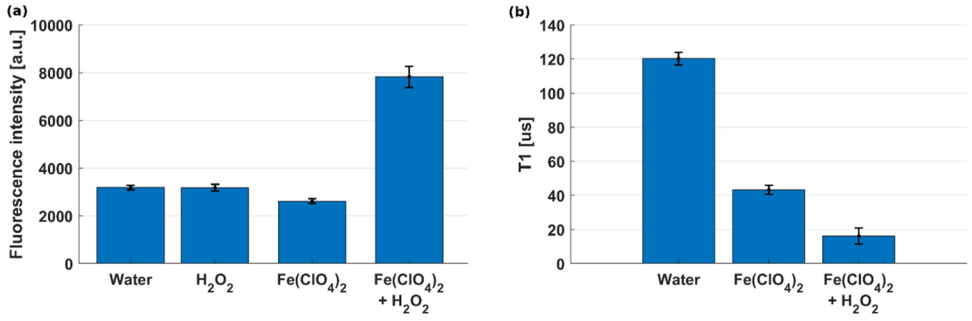

Figure 6. Determination of *OH and iron concentrations: (a) Results of a conventional kit to detect *OH (HPF). An increase in the *OH concentration leads to an increase in fluorescence ($|Fe(ClO_4)_2|$ = 100 μM, $|H_2O_2|$ = 1 mM). (b) Same measurements using NV centers in nanodiamonds and T1 relaxation time ($|Fe(ClO_4)_2|$ = 10 μM, $|H_2O_2|$ = 1 mM). The error bars show the standard error generated from three independent measurements on different particles.

Table 1. Overview of Standard Fluorescent Probes for Measuring Free Radicals

probe	mechanism	measure	sensitive for
HPF[37]	react with the species they detect and transform into a fluorescent form	what has been present between adding the dye and the time of measurement	reactive oxygen species
HTA[38]			*OH
DCFDA[39]			reactive oxygen species
Lucigenin[40]	emits chemiluminescence in the presence of ROS		reactive oxygen species mostly $*O^-$
FNDs (this work)	change T1 time in the presence of radicals	what is present now	spin noise (mostly from free radicals)

The first drop is associated with the presence of a paramagnetic form of iron in the sample. The second drop in the T1 value is explained by the generation of radicals in the sample, which proves that the sensitivity of relaxometry is sufficient to detect radicals, even when they coexist with other sources of magnetism. This measurement also demonstrates a useful feature of relaxometry: the ability to perform a measurement before and after a change. Having the ability to measure at the exact same spot on the exact same particle before and during the reaction gives a powerful control measurement. It is also important to point out that using the HPF probe required 14 h of incubation before a measurable fluorescent signal was obtained from the sample. The experiment using NV centers required only 20 min of acquisition. The acquisition time is restricted by the intensity of fluorescence of the ensemble of NV centers and the configuration of the relaxation experiment. It is possible to reduce the reported acquisition time and increase the time resolution of the experiment by reducing the number of repetitions and the number of dark times.

CONCLUDING REMARKS

In this article, we have investigated several aspects of relaxometry. We have shown that the sensitivity of NV centers to fluctuating spins depends on the size of the particle that hosts them (see Supporting Information, Figure S2). The study of NV performance under different conditions suggests that a protein corona interferes with measurement, while salts do not alter the outcome significantly. Despite this perturbation, it is remarkable that relaxometry determines a concentration of gadolinium as small as 1 nM. The determination of hydroxyl radical concentration in situ by means of NV centers demonstrates the potential of the technique as a sensor. For a comparison with other radical probes, we added Table 1.

While conventional probes suffer from bleaching (and thus can often only be measured in one shot), NV centers are almost infinitely stable and thus allow real-time determination over a long duration. We also showed that we can follow radical generation during a chemical reaction and that the determination is fully reversible. Additionally, since the method is a magnetic resonance method, it might be possible in the long run to differentiate between different radicals. Potentially, cross relaxation[41] or more complex pulsing schemes such as double electron−electron resonance (DEER)[42] offer this possibility. The most severe drawback of the presented technology is the large size of the diamond particles. Given that they are several tens of nanometers in size, the diamond particles are much larger than conventional radical probes. Apart from that, at least at this point, the method requires specialized homebuilt equipment, and the readout procedure is somewhat complicated. Since it is necessary to perform a pulsing sequence, the time that a measurement takes is considerably longer than measurement times with conventional dyes.

While so far chemicals have only been determined by diamond magnetometry in water, we take into account the presence of salts, glucose and proteins as components of the medium. We found that the formation of a protein corona in nanodiamonds influences sensing performance, while no differences are observed in the presence of salts. These experiments are essential for understanding and quantifying measurements in biological environments. Here, we also demonstrate diamond magnetometry measurements of free radicals, which are generated in situ in a chemical reaction for the first time. The concentrations that we are able to measure are definitely in a range that is interesting for investigating chemical reactions, as demonstrated here. Additionally, this measurement scheme is applicable for measurements in a biological environment. Here, the concentration varies greatly (values between nanomolar[43] and millimolar[44] concentrations have been estimated), and local concentrations are often

https://dx.doi.org/10.1021/acssensors.0c01037
ACS Sens. 2020, 5, 3862−3869

unknown. Compared to measurements with the conventional probe HPF, our T1 measurements provide real-time data rather than accumulating over the entire incubation period. While HPF required 14 h to reveal the concentration of *OH, we obtained a signal from an equivalent sample within a few minutes. Moreover, in the present experiments, we did not optimize the time resolution of the measurements; rather, we prioritized collecting complete T1 datasets. One could, for instance, decrease the number of dark times used in the pulse sequence. It is possible to deduce the relative change in T1 using a pulse sequence consisting of only one dark time. To do that, previous knowledge of the sample is necessary to choose the optimum length of the dark time. For example, the photolysis of H_2O_2 could be measured during one dark time of approximately 150 μs. This value maximizes the difference in intensity between the two cases (UV light on and off). Moreover, conventional chemical probes react irreversibly with radicals. NV centers, on the other hand, do not react with radicals and thus offer reversibility. Finally, we surprisingly found that smaller nanodiamonds show higher T1 times for particles containing dense ensembles.

■ ASSOCIATED CONTENT

Supporting Information

The Supporting Information is available free of charge at https://pubs.acs.org/doi/10.1021/acssensors.0c01037.

Measurements of particles of different sizes; full T1 curves; details on data fitting; control measurements for the UV experiment without H_2O_2; and measurements with HTA for comparison (PDF)

■ AUTHOR INFORMATION

Corresponding Authors

Mayeul Chipaux − *Institute of Physics, École Polytechnique Fédérale de Lausanne (EPFL), CH-1015 Lausanne, Switzerland*; Email: Mayeul.chipaux@epfl.ch

Romana Schirhagl − *Department of Biomedical Engineering, University Medical Center Groningen, Groningen University, 9713 AW Groningen, The Netherlands*; orcid.org/0000-0002-8749-1054; Email: Romana.schirhagl@gmail.com

Authors

Felipe Perona Martínez − *Department of Biomedical Engineering, University Medical Center Groningen, Groningen University, 9713 AW Groningen, The Netherlands*; orcid.org/0000-0001-8759-9586

Anggrek Citra Nusantara − *Department of Biomedical Engineering, University Medical Center Groningen, Groningen University, 9713 AW Groningen, The Netherlands*

Sandeep Kumar Padamati − *Department of Biomedical Engineering, University Medical Center Groningen, Groningen University, 9713 AW Groningen, The Netherlands*

Complete contact information is available at: https://pubs.acs.org/10.1021/acssensors.0c01037

Author Contributions

§F.P.M. and A.C.N. contributed equally to this work.

Notes

The authors declare no competing financial interest.

■ ACKNOWLEDGMENTS

R.S. acknowledges financial support from FOM via the Projectruimte Grant 15PR3229 and from the ERC Starting Grant 714289—Stress Imaging. F.P.M. acknowledges support from the Chilean Government via a CONICYT scholarship (Grant Number 72160222). The authors thank Prof. Wesley R. Browne from the Stratingh Institute for Chemistry for kindly giving them access to a fluorometer.

■ REFERENCES

(1) Rondin, L.; Tetienne, J. P.; Hingant, T.; Roch, J. F.; Maletinsky, P.; Jacques, V. Magnetometry with Nitrogen-Vacancy Defects in Diamond. *Rep. Prog. Phys.* **2014**, *77*, No. 056503.

(2) Schirhagl, R.; Chang, K.; Loretz, M.; Degen, C. L. Nitrogen-Vacancy Centers in Diamond: Nanoscale Sensors for Physics and Biology. *Annu. Rev. Phys. Chem.* **2014**, *65*, 83−105.

(3) Glenn, D. R.; Fu, R. R.; Kehayias, P.; Le Sage, D.; Lima, E. A.; Weiss, B. P.; Walsworth, R. L. Micrometer-Scale Magnetic Imaging of Geological Samples Using a Quantum Diamond Microscope. *Geochem., Geophys. Geosyst.* **2017**, *18*, 3254−3267.

(4) Stürner, F. M.; Brenneis, A.; Kassel, J.; Wostradowski, U.; Rölver, R.; Fuchs, T.; Nakamura, K.; Sumiya, H.; Onoda, S.; Isoya, J.; Jelezko, F. Compact Integrated Magnetometer Based on Nitrogen-Vacancy Centers in Diamond. *Diamond Relat. Mater.* **2019**, *93*, 59−65.

(5) Chipaux, M.; Toraille, L.; Larat, C.; Morvan, L.; Pezzagna, S.; Meijer, J.; Debuisschert, T. Wide Bandwidth Instantaneous Radio Frequency Spectrum Analyzer Based on Nitrogen Vacancy Centers in Diamond. *Appl. Phys. Lett.* **2015**, *107*, No. 233502.

(6) Nowodzinski, A.; Chipaux, M.; Toraille, L.; Jacques, V.; Roch, J. F.; Debuisschert, T. Nitrogen-Vacancy Centers in Diamond for Current Imaging at the Redistributive Layer Level of Integrated Circuits. *Microelectron. Reliab.* **2015**, *55*, 1549−1553.

(7) Hemelaar, S. R.; de Boer, P.; Chipaux, M.; Zuidema, W.; Hamoh, T.; Perona Martinez, F.; Nagl, A.; Hoogenboom, J. P.; Giepmans, B. N. G.; Schirhagl, R. Nanodiamonds as Multi-Purpose Labels for Microscopy. *Sci. Rep.* **2017**, *7*, No. 720.

(8) Nagarajan, S.; Pioche-Durieu, C.; Tizei, L. H. G.; Fang, C. Y.; Bertrand, J. R.; Le Cam, E.; Chang, H. C.; Treussart, F.; Kociak, M. Simultaneous Cathodoluminescence and Electron Microscopy Cytometry of Cellular Vesicles Labeled with Fluorescent Nanodiamonds. *Nanoscale* **2016**, *8*, 11588−11594.

(9) Chipaux, M.; van der Laan, K.; Hemelaar, S. R.; Hasani, M.; Zheng, T.; Schirhagl, R. Nanodiamonds and Their Applications in Cells. *Small* **2018**, *14*, No. 1704263.

(10) van der Laan, K.; Hasani, M.; Zheng, T.; Schirhagl, R. Nanodiamonds for In Vivo Applications. *Small* **2018**, No. 1703838.

(11) Grinolds, M. S.; Hong, S.; Maletinsky, P.; Luan, L.; Lukin, M.; Walsworth, R. L.; Yacoby, A. Nanoscale Magnetic Imaging of a Single Electron Spin under Ambient Conditions. *Nat. Phys.* **2013**, *9*, 215−219.

(12) Zopes, J.; Cujia, K. S.; Sasaki, K.; Boss, J. M.; Itoh, K. M.; Degen, C. L. Three-Dimensional Localization Spectroscopy of Individual Nuclear Spins with Sub-Angstrom Resolution. *Nat. Commun.* **2018**, *9*, No. 4678.

(13) Mamin, H. J.; Kim, M.; Sherwood, M. H.; Rettner, C. T.; Ohno, K.; Awschalom, D. D.; Rugar, D. Nanoscale Nuclear Magnetic Resonance with a Nitrogen-Vacancy Spin Sensor. *Science* **2013**, *339*, 557−560.

(14) Rondin, L.; Tetienne, J. P.; Rohart, S.; Thiaville, A.; Hingant, T.; Spinicelli, P.; Roch, J. F.; Jacques, V. Stray-Field Imaging of Magnetic Vortices with a Single Diamond Spin. *Nat. Commun.* **2013**, *4*, No. 2279.

(15) Pelliccione, M.; Jenkins, A.; Ovartchaiyapong, P.; Reetz, C.; Emmanouilidou, E.; Ni, N.; Bleszynski Jayich, A. C. Scanned Probe Imaging of Nanoscale Magnetism at Cryogenic Temperatures with a Single-Spin Quantum Sensor. *Nat. Nanotechnol.* **2016**, *11*, 700−705.

(16) Rondin, L.; Tetienne, J. P.; Spinicelli, P.; Dal Savio, C.; Karrai, K.; Dantelle, G.; Thiaville, A.; Rohart, S.; Roch, J. F.; Jacques, V.

Nanoscale Magnetic Field Mapping with a Single Spin Scanning Probe Magnetometer. *Appl. Phys. Lett.* **2012**, *100*, No. 153118.
(17) Tetienne, J. P.; Lombard, A.; Simpson, D. A.; Ritchie, C.; Lu, J.; Mulvaney, P.; Hollenberg, L. C. L. Scanning Nanospin Ensemble Microscope for Nanoscale Magnetic and Thermal Imaging. *Nano Lett.* **2016**, *16*, 326−333.
(18) Lovchinsky, I.; Sushkov, A. O.; Urbach, E.; De Leon, N. P.; Choi, S.; De Greve, K.; Evans, R.; Gertner, R.; Bersin, E.; Muller, C.; McGuinness, L. P.; Jelezko, F.; Walsworth, R. L.; Park, H.; Lukin, M. Nuclear Magnetic Resonance Detection and Spectroscopy of Single Proteins Using Quantum Logic. *Science* **2016**, *351*, 836−841.
(19) Devience, S. J.; Pham, L. M.; Lovchinsky, I.; Sushkov, A. O.; Bar-Gill, N.; Belthangady, C.; Casola, F.; Corbett, M.; Zhang, H.; Lukin, M.; Park, H.; Yacoby, A.; Walsworth, R. L. Nanoscale NMR Spectroscopy and Imaging of Multiple Nuclear Species. *Nat. Nanotechnol.* **2015**, *10*, 129−134.
(20) Steinert, S.; Ziem, F.; Hall, L. T.; Zappe, A.; Schweikert, M.; Götz, N.; Aird, A.; Balasubramanian, G.; Hollenberg, L.; Wrachtrup, J. Magnetic Spin Imaging under Ambient Conditions with Sub-Cellular Resolution. *Nat. Commun.* **2013**, *4*, No. 1607.
(21) Simpson, D. A.; Ryan, R. G.; Hall, L. T.; Panchenko, E.; Drew, S. C.; Petrou, S.; Donnelly, P. S.; Mulvaney, P.; Hollenberg, L. C. L. Electron Paramagnetic Resonance Microscopy Using Spins in Diamond under Ambient Conditions. *Nat. Commun.* **2017**, *8*, No. 458.
(22) Mrózek, M.; Rudnicki, D.; Kehayias, P.; Jarmola, A.; Budker, D.; Gawlik, W. Longitudinal Spin Relaxation in Nitrogen-Vacancy Ensembles in Diamond. *EPJ Quantum Technol.* **2015**, *2*, No. 22.
(23) Ariyaratne, A.; Bluvstein, D.; Myers, B. A.; Jayich, A. C. B. Nanoscale Electrical Conductivity Imaging Using a Nitrogen-Vacancy Center in Diamond. *Nat. Commun.* **2018**, *9*, No. 2406.
(24) Sushkov, A. O.; Chisholm, N.; Lovchinsky, I.; Kubo, M.; Lo, P. K.; Bennett, S. D.; Hunger, D.; Akimov, A.; Walsworth, R. L.; Park, H.; Lukin, M. All-Optical Sensing of a Single-Molecule Electron Spin. *Nano Lett.* **2014**, *14*, 6443−6448.
(25) Kaufmann, S.; Simpson, D. A.; Hall, L. T.; Perunicic, V.; Senn, P.; Steinert, S.; McGuinness, L. P.; Johnson, B. C.; Ohshima, T.; Caruso, F.; Wrachtrup, J.; Scholten, R. E.; Mulvaney, P.; Hollenberg, L. Detection of Atomic Spin Labels in a Lipid Bilayer Using a Single-Spin Nanodiamond Probe. *Proc. Natl. Acad. Sci. U.S.A.* **2013**, *110*, 10894−10898.
(26) Chen, X.; Tian, X.; Shin, I.; Yoon, J. Fluorescent and Luminescent Probes for Detection of Reactive Oxygen and Nitrogen Species. *Chem. Soc. Rev.* **2011**, *40*, 4783−4804.
(27) Morita, A.; Hamoh, T.; Perona Martinez, F.; Chipaux, M.; Sigaeva, A.; Mignon, C.; van der Laan, K. J.; Hochstetter, A.; Schirhagl, R. The Fate of Lipid-Coated and Uncoated Fluorescent Nanodiamonds during Cell Division in Yeast. *Nanomaterials* **2020**, *10*, No. 516.
(28) Freinbichler, W.; Colivicchi, M. A.; Fattori, M.; Ballini, C.; Tipton, K. F.; Linert, W.; Della Corte, L. Validation of a Robust and Sensitive Method for Detecting Hydroxyl Radical Formation Together with Evoked Neurotransmitter Release in Brain Microdialysis. *J. Neurochem.* **2008**, *105*, 738−749.
(29) Ermakova, A.; Pramanik, G.; Cai, J. M.; Algara-Siller, G.; Kaiser, U.; Weil, T.; Tzeng, Y. K.; Chang, H. C.; McGuinness, L. P.; Plenio, M. B.; Naydenov, B.; Jelezko, F. Detection of a Few Metallo-Protein Molecules Using Color Centers in Nanodiamonds. *Nano Lett.* **2013**, *13*, 3305−3309.
(30) Tetienne, J. P.; Hingant, T.; Rondin, L.; Cavaill, A.; Mayer, L.; Dantelle, G.; Gacoin, T.; Wrachtrup, J.; Roch, J. F.; Jacques, V. Spin Relaxometry of Single Nitrogen-Vacancy Defects in Diamond Nanocrystals for Magnetic Noise Sensing. *Phys. Rev. B* **2013**, *87*, No. 235436.
(31) Rioux, J. A.; Levesque, I. R.; Rutt, B. K. Biexponential Longitudinal Relaxation in White Matter: Characterization and Impact on T1 Mapping with IR-FSE and MP2RAGE. *Magn. Reson. Med.* **2016**, *75*, 2265−2277.
(32) Manson, N. B.; Hedges, M.; Barson, M. S. J.; Ahlefeldt, R.; Doherty, M. W.; Abe, H.; Ohshima, T.; Sellars, M. J. NV–N+ Pair Centre in 1b Diamond. *New J. Phys.* **2018**, *20*, No. 113037.
(33) Hemelaar, S. R.; Nagl, A.; Bigot, F.; Rodríguez-García, M. M.; de Vries, M. P.; Chipaux, M.; Schirhagl, R. The Interaction of Fluorescent Nanodiamond Probes with Cellular Media. *Microchim. Acta* **2017**, *184*, 1001−1009.
(34) Merz, V.; Lenhart, J.; Vonhausen, Y.; Ortiz-Soto, M. E.; Seibel, J.; Krueger, A. Zwitterion-Functionalized Detonation Nanodiamond with Superior Protein Repulsion and Colloidal Stability in Physiological Media. *Small* **2019**, *15*, No. 1901551.
(35) Valko, M.; Rhodes, C. J.; Moncol, J.; Izakovic, M.; Mazur, M. Free Radicals, Metals and Antioxidants in Oxidative Stress-Induced Cancer. *Chem.−Biol. Interact.* **2006**, *160*, 1−40.
(36) Kruszewski, M. Labile Iron Pool: The Main Determinant of Cellular Response to Oxidative Stress. *Mutat. Res.* **2003**, *531*, 81−92.
(37) Tomizawa, S.; Imai, H.; Tsukada, S.; Simizu, T.; Honda, F.; Nakamura, M.; Nagano, T.; Urano, Y.; Matsuoka, Y.; Fukasaku, N.; Saito, N. The Detection and Quantification of Highly Reactive Oxygen Species Using the Novel HPF Fluorescence Probe in a Rat Model of Focal Cerebral Ischemia. *Neurosci. Res.* **2005**, *53*, 304−313.
(38) Qu, X.; Kirschenbaum, L. J.; Borish, E. T. Hydroxyterephthalate as a Fluorescent Probe for Hydroxyl Radicals: Application to Hair Melanin. *Photochem. Photobiol.* **2000**, *71*, 307−313.
(39) Sundaresan, M.; Yu, Z. X.; Ferrans, V. J.; Irani, K.; Finkel, T. Requirement for Generation of H2O2 for Platelet-Derived Growth Factor Signal Transduction. *Science* **1995**, *270*, 296−299.
(40) Faulkner, K.; Fridovich, I. Luminol and Lucigenin as Detectors for O2ṡ-. *Free Radical Biol. Med.* **1993**, *15*, 447−451.
(41) Wood, J. D. A.; Tetienne, J. P.; Broadway, D. A.; Hall, L. T.; Simpson, D. A.; Stacey, A.; Hollenberg, L. C. L. Microwave-Free Nuclear Magnetic Resonance at Molecular Scales. *Nat. Commun.* **2017**, *8*, No. 15950.
(42) Kim, M.; Mamin, H. J.; Sherwood, M. H.; Ohno, K.; Awschalom, D. D.; Rugar, D. Decoherence of Near-Surface Nitrogen-Vacancy Centers Due to Electric Field Noise. *Phys. Rev. Lett.* **2015**, *115*, No. 087602.
(43) Rahman, K. Studies on Free Radicals, Antioxidants, and Co-Factors. *Clin. Interventions Aging* **2007**, *2*, 219−236.
(44) Paardekooper, L. M.; Dingjan, I.; Linders, P. T. A.; Staal, A. H. J.; Cristescu, S. M.; Verberk, W. C. E. P.; Van Den Bogaart, G. Human Monocyte-Derived Dendritic Cells Produce Millimolar Concentrations of ROS in Phagosomes per Second. *Front. Immunol.* **2019**, *10*, No. 1216.

https://dx.doi.org/10.1021/acssensors.0c01037
ACS Sens. 2020, 5, 3862−3869